Appl. Phys. A (2017) 123:482
DOI 10.1007/s00339-017-1097-9

Applied Physics A
Materials Science & Processing

Isotopic enrichment of Zn particles by laser ablation

Marcelo N. Felix Pozzi[1] · Gonzalo Guidali[1] · Mauricio Fernández[2] · Erica Zubillaga[2] · Carlos A. Rinaldi[1,3,4]

Received: 15 March 2017 / Accepted: 16 June 2017

Abstract The use of Zn in nuclear reactors reduces the amount of ^{60}Co generated as a consequence of the natural activation of Co. On the other hand, isotopically enriched Zn can be used as a tracer in biological systems. At the present, the enrichment of Zn is obtained using gaseous compounds of the metal by centrifugal force. In this paper, we present a method based on laser ablation of metallic targets of Zn with a Nd–YAG nanosecond laser to produce isotopically enriched Zn particles. Also, the effect of the wavelength irradiation laser on the enrichment factor was studied and a procedure is proposed to collect the different enrichment fractions yield.

1 Introduction

Zinc reduces the amount of radioactive ^{60}Co formed as a consequence of the activation of natural Co in the construction materials of the reactor. ^{60}Co is a major contributor to radiation build-up in the cooling systems, and therefore, also causes elevated dose rates of maintenance personnel. If natural Zn is injected, ^{64}Zn forms the radioactive ^{65}Zn which negates the beneficial reduction of ^{60}Co level. If the ^{64}Zn isotope is removed prior to injection in the cooling system, full advantage can be taken from the ^{60}Co level reduction and the average dose rates are substantially reduced. On the other hand, the ubiquitous presence of Zn in the environment limits the ability to study its bioaccumulation dynamics upon short time exposures to environmentally realistic concentrations [1]. However, these limitations can be overcome using stable isotope labeled nanoparticles. Gulson et al. [2] suggested that stable isotopes tracing may prove valuable for monitoring nanoparticles in the field and addressing emerging research questions. Dybowska et al. [3] demonstrated that it is possible to synthesize isotopically modified ZnO nanoparticles that are suitable as biological/environmental nanotoxicity tracer. These, among other reasons, are the basis for developing a process of separation of zinc isotopes. Current centrifugal isotopic separation systems require the use of these elements in a gaseous form like diethyl Zn, which is toxic and flammable. Another technology that could be used is the isotopic separation induced by laser ablation [4, 5].

The modern techniques of pulsed laser deposition (PLD) are based on the interaction of laser light with the surface of a material, leading to a detachment of electrons, ions, molecules and even small pieces of the material of that surface. The objective of this work is the characterization on the measurement of the diameter and the elemental isotope ratio of particles deposited on the surfaces target. According to experiments carried out on different metals [6], the spatial distribution of the particles leaking from the ablation, continue a relationship trigonometric powers, whose expression is:

✉ Carlos A. Rinaldi
rinaldi@cnea.gov.ar

[1] Departamento de Micro y Nanotecnología, Centro Atómico Constituyentes, Comisión Nacional de Energía Atómica, San Martín, Buenos Aires, Argentina

[2] Gerencia Química, Centro Atómico Constituyentes, Comisión Nacional de Energía Atómica, San Martín, Buenos Aires, Argentina

[3] Escuela de Ciencia y Tecnología, Universidad Nacional de San Martín, San Martín, Buenos Aires, Argentina

[4] Consejo Nacional de Investigaciones Científicas y Técnicas, Buenos Aires, Argentina

Published online: 22 June 2017

$$f = f_0 \times \cos^n \theta \quad (1)$$

where f is the flow of cone ablation, θ the angle respect to the normal irradiated surface, f_0 is the flow of particles ejected from the normal surface and n, an experimental factor whose value has not yet been able to be clarified how it relates to different parameters of the setup [7]. The particles deposited on the surface have morphology and dimensions that depend on the energy of the beam, the heat capacity of the ablated material and its Debye temperature [8]. Also, the isotopic separation was observed during ablation of standard copper samples by a nanosecond Nd–YAG laser and a femtosecond Ti; sapphire laser at 266 nm [9] and a mechanism based on the electric field interactions between the electrons and ions is proposed to explain the separation of isotopes in the plume. On the other hand, a highly efficient isotope enrichment process is observed directly in laser ablation plumes generated from ultrafast laser pulses focused on a solid surface and a plasma centrifuge mechanism is proposed as a reasonable explanation of the results [10]. Taking into account this latest technology, this work carried out a study of the conditions necessary for the production of isotopically enriched Zn particles.

2 Experimental setup

An image of the experimental setup is shown in Fig. 1. It consists of a laser, a vacuum chamber with a motorized stage. Two different Nd–YAG lasers were used for irradiating the samples; one laser delivered a 9-ns pulse of 450 mJ at 1064 nm at the repetition rate of 10 Hz and another one laser delivered a 9-ns pulse of 125 mJ at 266 nm at the same repetition rate. The laser beam was focused to a 1-mm diameter spot on the target surface using a 75 mm focal length lens. Under these experimental conditions, the laser energy was maintained constant in the range of 100–125 mJ. The sample was a piece of Zn (ACS reagent, reag. ISO, reag. Ph. Eur., Purity $\geq$ 99.9%) that was fixed to a target axis in a vacuum chamber at 0.016 Torr of total pressure.

This value was needed to obtain a long ablation plume for the spatial distribution. A schematic view of the ablation chamber is shown in Fig. 2.

The distance between the ablation target and the set of concentric discs (M1, M2, and M3) can be described with a conical geometry whose angles are related as it is shown in Fig. 3. The values for the angles obtained by these rings are $\Delta\theta_1 = 8.1°$, $\Delta\theta_2 = 8.1°$ and $\Delta\theta_3 = 10.4°$.

The laser emission of different wavelengths (1064, 532 and 266 nm) was focused on a surface target of Zn during 10 min at 10 Hz and particles ejected from the substrate were collected on the concentric discs to determine the different particle sizes and their different isotopic composition. To perform SEM and TIM analyzes, depositions were made on Teflon discs and stainless steel discs under the same experimental conditions. After the deposition of the particles, they were extracted and stored in three small individual boxes for transport to a SEM microscope (stainless steel discs) and performing analysis of corresponding isotopic composition (Teflon discs). Table 1 shows the results obtained for the different ablation wavelengths with their corresponding α (enrichment factor) and Fig. 4 show a SEM image with a typical particle size distribution for 266 nm laser irradiation wavelength.

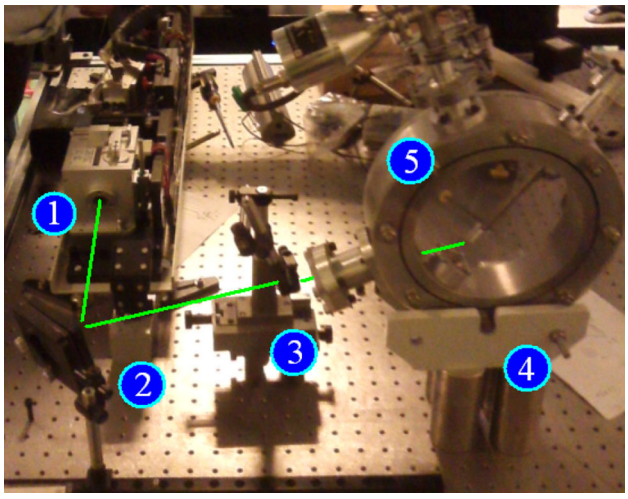

Fig. 1 Image of the experimental setup. *1* Nd:YAG pulsed laser, *2* plane mirror, *3* focal lens, *4* support to fix the A.C., and *5* ablation chamber (AC)

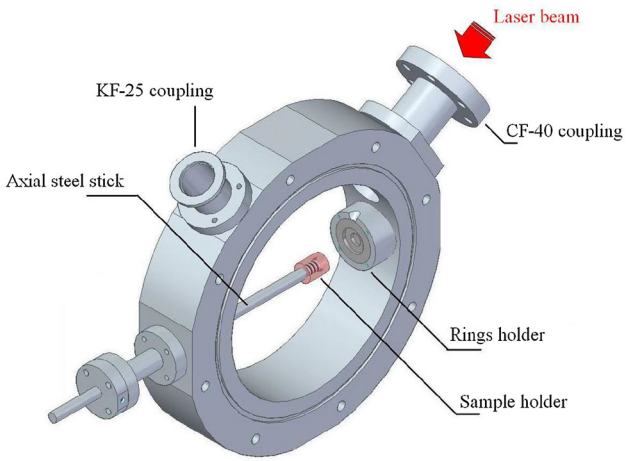

Fig. 2 Detail of the ablation chamber. The *red arrow* indicates the direction of the laser beam. **a** Target sample (inside the "sample holder"), **b** Rings for collecting the ablation products (inside the "rings holder")

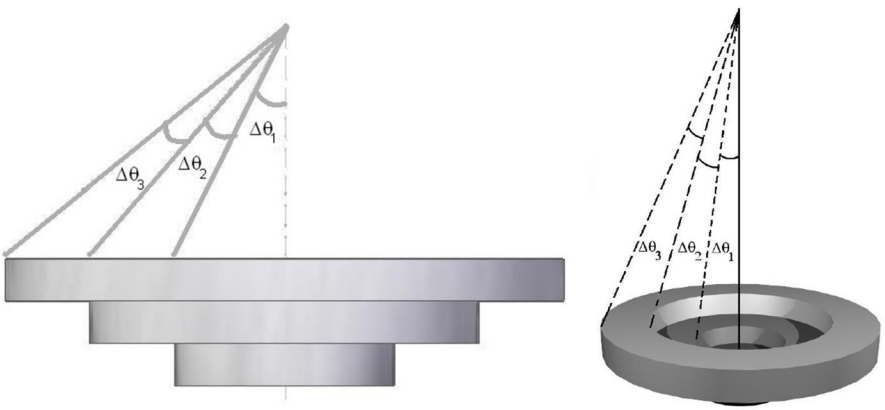

Fig. 3 Rings collector system. **a** Lateral schematic view **b** isometric schematic view. Observe the differences angular collection given by the geometry of the system

Table 1 Ring zone angle deposition, laser wavelength irradiation, the ratio of Zn isotopes and degree of enrichment of deposited ablation plume

Ring zone	λ (nm)	Isotope	Isotopic ratio	Alpha (α)
M3($\Delta\theta_3$)	266	64/66	1.789 ± 0.005	1.0205
		66/68	1.524 ± 0.001	1.0073
	532	64/66	1.764 ± 0.005	1.0063
		66/68	1.504 ± 0.001	0.9940
	1064	64/66	1.747 ± 0.005	0.9966
		66/68	1.495 ± 0.001	0.9881
M2($\Delta\theta_2$)	266	64/66	1.778 ± 0.005	1.0247
		66/68	1.515 ± 0.001	1.0013
	532	64/66	1.777 ± 0.005	1.0240
		66/68	1.504 ± 0.001	0.9940
	1064	64/66	1.747 ± 0.005	1.0069
		66/68	1.492 ± 0.001	0.9861
M1($\Delta\theta_1$)	266	64/66	1.774 ± 0.005	1.0120
		66/68	1.513 ± 0.001	1.0000
	532	64/66	1.761 ± 0.005	1.0045
		66/68	1.502 ± 0.001	0.9930
	1064	64/66	1.743 ± 0.005	0.9943
		66/68	1.486 ± 0.001	0.9821

3 Results and discussions

3.1 Isotopic analysis

Thermal ionization mass spectrometry (TIMS) is the reference technique to validate isotopic composition of metals in solid samples. The instrument has a magnetic analyzer that provides flat peaks and simultaneous collection (multicollector) of different beams of all isotopes of the element ions, avoiding fluctuations due to signal instability. Both features contribute to being the most precise and accurate mass spectrometry technique [11–13]. Despite increased analysis time and the particular sample pre-treatment, it has an expanded relative uncertainty of 0.05–0.5% for measurements of isotopic ratios of Zn. The ability to see a noticeable natural isotopic fractionation of Zn depends critically on the accuracy of measurements. Zinc is a relatively volatile metal in thermal processes. Its first ionization potential is (9.39 eV) and its melting point is relatively low (419.58 °C). Its efficient ionization is complicated; the addition of a suspension of silica gel and deposited on rhenium filaments where the sample, dissolved in phosphoric acid, produces a glassy emitter, generating a more stable and reproducible signal. Metal Zn samples coming from laser-pulsed deposition on PTFE rings, were dissolved in about 10 mL of 3 M HNO_3 by heating under boiling point and then evaporated to a minimum volume of about 0.5 mL. 5 µL of the solution was deposited on a rhenium filament (double filament configuration) and dried electrically. Then, a drop of silica suspension is added on sample deposit and dried again. Finally, a drop of concentrated orthophosphoric acid followed by electrical drying is added also to the sample with silica. In this way, the sample is now ready to enter the TIMS for isotopic analysis [14]. The results obtained by this procedure are shown in Table 1.

3.2 SEM analysis

Observing the results given in Table 1, it can be seen that the greatest enrichment effect is obtained by irradiating with the laser at 266 nm. For this reason, it was realized a study of the size of the particles deposited in the central ring (M1 ($\Delta\theta_1$)) and in the outer ring (M3 ($\Delta\theta_3$)). SEM analysis was performed using FEI SEM Quanta 200. The images obtained in TIFF format were digitally processed to eliminate the substrate background effect where the particles were deposited. The results obtained are shown in Figs. 4 and 5. From these images and using the image processing software ImageJ [15], the particles size distributions were obtained. The distributions for both samples (M1 and M3) were fitted using the following Gaussian distribution function:

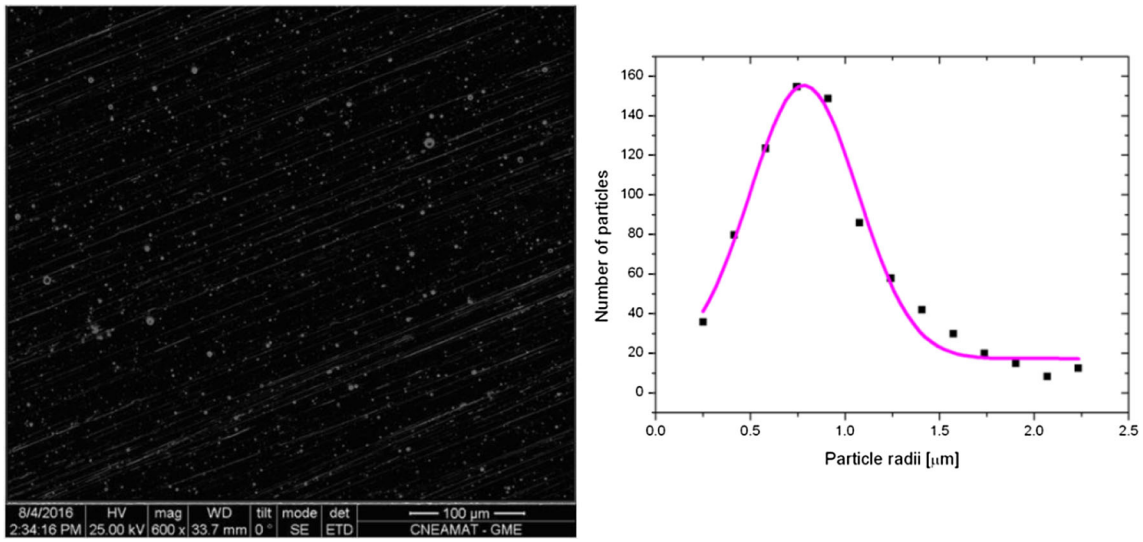

Fig. 4 SEM image and particles distribution for the M1 collect ring ($\Delta\theta_1$) at 266 nm laser ablation wavelength

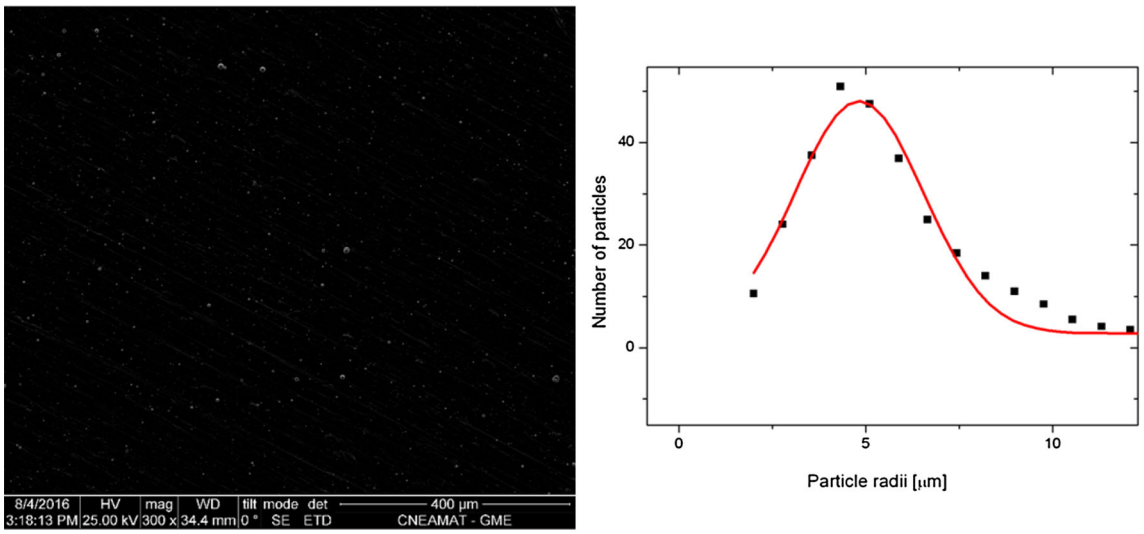

Fig. 5 SEM image and particles distribution for the M3 collect ring ($\Delta\theta_3$) at 266 nm laser ablation wavelength

$$y = y_0 + \frac{A}{\omega\sqrt{\pi/2}} e^{-2\left(\frac{x-x_c}{\omega}\right)^2} \quad (2)$$

where X_c is the radii of the particle, and ω is the spread of the distribution. The parameters for the distribution functions are shown in Table 2. The fitting results are shown in Figs. 4 and 5 together with the corresponding SEM image.

The results indicate that in the central ring ($\Delta\theta_1$) the particles with an average radius of 800 nm are deposited, while in the outer ring ($\Delta\theta_3$) the particles have an average radius of 4.8 µm.

The bibliography shows that shorter wavelengths provide higher photon energies for bond breaking (molecules) and the ionization process. Moreover, the mass-ablation rate varies [16] with excitation wavelength as $\lambda^{-4/9}$. Hence

Table 2 Parameters of Gaussian regression for the collector ring zone particles size distribution

Ring zone	Parameter	Value (µm)
M3 ($\Delta\theta_3$)	y_0	2.8 ± 0.8
	X_c	4.8 ± 0.1
	ω	3.4 ± 0.2
	A	194 ± 10
M1 ($\Delta\theta_1$)	y_0	17.2 ± 3.7
	X_c	0.8 ± 0.0
	ω	0.6 ± 0.0
	A	99 ± 7

laser–target coupling efficiency will be higher for shorter wavelength excitation [17]. On the other hand, in the same work [17] it is shown that the irradiation wavelength produces ions with wider energy distributions as the wavelength decreases. This broadening is attributed to the enhanced three-body recombination in dense shorter wavelength plasmas. In our case, these results clearly indicate that the wavelength increases the ion concentration to 266 nm giving rise to larger particles that deposit in the outermost zone of the plume ($\Delta\theta_3$) with a higher 64/66 isotopic ratio. The lighter atom goes towards the outside of the plume but the smallest particles deposit in the central zone of the plume ($\Delta\theta_1$) with a lower ratio 64/66 than in outer zone ($\Delta\theta_3$) (See Table 1). These results indicate that the kinetics of particle formation [18–21] is subsequent to the isotopic enrichment process. This fact implies that a centrifugal plasma process [22] would be carried out that changes the ratio of isotopes and later, these atoms are added forming the particles that are deposited in the different zones. When comparing these results with those obtained with femtosecond laser ablation at 780 nm [5] the mechanism seems inverted. In that case, the lighter atom travels to the center of the ablation plume and the centrifugal plasma process seems to dominate.

From the data obtained that are observed in Table 1, there are two mechanisms that control the process of isotopic enrichment that depend on the wavelength of laser irradiation. The first, a fluid dynamics control, when performing the laser ablation process at 1064 nm leads to heavier atoms towards the center of the pen and the enrichment factor (α) is smaller in the central ring ($\Delta\theta_1$). In the second case, when ablation is performed at 266 nm the effect of centrifugal plasma due to the high concentration of ions leads to the lighter atoms in the central zone of the pen and the enrichment factor (α) is greater in the central ring ($\Delta\theta_1$). On the other hand, in the case of the particles generation at 266 nm due to the high ion density, the wide distribution of their velocities and their angular distribution, the nucleation produces larger particles in the external part of the plume, as it is shown in Fig. 5. In this way, larger particles (5 μ R) can be obtained, with high enrichment factor (α) and smaller particles (800 nm R) with low enrichment factor (α).

4 Conclusions

These results clearly indicate that the shorter wavelength increases the ion concentration and a centrifugal effect would increase the isotopic separation effect. See the alpha (α) enrichment factor on Table 1. The ion concentration is greater at the shortest wavelength and the kinetics of particle formation follows the separation process. The method used in this work allows produces isotopically enriched Zn particles, controlling the size and the alpha factor. The enrichment factor is higher than in the diffusion systems but smaller than the centrifuge considering a cascade system. From these results, it is possible to determine that the system allows the separation of isotopes in degrees of enrichment variable depending on the area of the ablation plume used to collect the products. However, it is not necessary to use the isotopes in a gas state in order to make the separation process and in this way, it could reduce the cost of production. For this process, it is possible to use basically any high power nanosecond laser but different wavelengths will produce different enrichment factor (α).

Acknowledgements The authors gratefully acknowledge financial support from the Consejo Nacional de Investigaciones Científicas y Tecnológicas (CONICET), the University of San Martín (UNSAM), Buenos Aires, and the Comisión Nacional de Energía Atómica (CNEA) from Argentina.

References

1. S.N. Luoma, P.S. Rainbow, Why is metal bioaccumulation so variable? Biodynamics as a unifying concept. Environ. Sci. Technol. **39**(7), 1921–1931 (2005)
2. B. Gulson, H. Wong, Stable isotopic tracing a way forward for nanotechnology. Environ. Health Perspect. **114**(10), 1486–1488 (2006)
3. A.D. Dybowska, M. Croteau, K.M. Superb, D. Berhanu, S.N. Luoma, P. Christian, P. O'Brien, E. Valsami-Jones, Environ. Pollut. **159**, 266–273 (2011)
4. M. Joseph, P. Manoravi, Appl. Phys. A **76**, 153 (2003)
5. P. Vanrompay, Z. Zhang, J. Nees, P. Pronko, C. Science, A. Arbor, Isotope separation and enrichment by ultrafast laser ablation. Proc. SPIE **3934**, 43–51 (2000)
6. K.L. Saenger, J. Appl. Phys. **70**, 5629 (1991). doi:10.1063/1.350178
7. D. Ali, M.Z. Butt, M. Khaleeq-ur-Rahman, Appl. Surf. Sci. **257**(7), 2854–2860 (2011)
8. Majid Vaezzadeh, Mohammadreza Saeidi, Mohsen Zarei, Phys. E **42**, 1787–1789 (2010)
9. Timothy Wu Suen, Xianglei Mao, and Richard E. Russo, CP1278, International Symposium on High Power Laser Ablation 2010, edited by C. R. Phipps © 2010 American Institute of Physics 978-0-7354-0828-9/10/330.00
10. P.P. Pronko, P.A. VanRompay, Z. Zhang, J.A. Nees, Phys. Rev. Lett. **83**, 13 (1999)
11. M. Janghorbani, B. Ting, J. Nutr. Biochem. **1**, 4–19 (1990)
12. F. Adams, R. Gijbels, R. Van Grieken (eds.), *Inorganic Mass Spectrometry* (Wiley, New York, 1988)
13. J.R. Turnland, J. Nutr. **119**(1), 7–14 (1989)
14. E. Gautier, M. Bavio, M. Fernández, Anal. Methods **7**, 10452–10456 (2015)
15. C.A. Schneider, W.S. Rasband, K.W. Eliceiri, NIH Image to ImageJ: 25 years of image analysis. Nat. Methods **9**, 671–675 (2012)
16. R.A. Burdt, S. Yuspeh, K.L. Sequoia, Y.Z. Tao, M.S. Tillack, F. Najmabadi, J. Appl. Phys. **106**, 033310 (2009)
17. J.R. Freeman, S.S. Harilal, B. Verhoff, A. Hassanein, B. Rice, Plasma Sources Sci. Technol. **21**, 055003 (2012)
18. M. Vaezzadeh, M. Saeidi, M. Zarei, Phys. E **42**, 1787–1789 (2010)

19. M. Girault, L. Hallo, L. Lavisse, M.M. De Lucas, D. Hebert, V. Potin, J.M. Jouvard, Appl. Surf. Sci. **258**, 9461–9465 (2012)
20. A. Cazzaniga, R.B. Ettlinger, S. Canulescu, J. Schou, N. Pryds, Appl. Phys. A **117**, 89–92 (2014)
21. P.P. Pronko, P.A. VanRompay, Z. Zhang, J.A. Nees, Phys. Rev. Lett. **83**(13), 2596–2599 (1999)
22. V. Dudoitis, V. Ulevičius, G. Račiukaitis, N. Špirkauskaitė, K. Plauškaitė, Lith. J. Phys. **51**, 248–259 (2011)